Systems & Control Transactions

Original Research Article
Peer Reviewed Conference Proceeding
ESCAPE 36 - European Symposium on Computer Aided Process Engineering
Sheffield, UK. 21-24 June 2026

PSE PRESS

Accelerating Design of Chemical Recycling of Plastic Waste through Digitalization: A Bubbling Fluidized Bed Reactor Case Study

Stefano Iannello*, Vassilis M. Charitopoulos, Massimiliano Materazzi

University College London, Department of Chemical Engineering, Torrington Place, London WC1E 7JE, UK
* Corresponding Author: stefano.iannello.18@ucl.ac.uk.

ABSTRACT

The reliable identification of feasible and optimal operating conditions is a key challenge in the design and optimization of thermochemical conversion processes, where kinetics, limited data availability, and strict physical constraints coexist. In this work, a novel data-driven strategy based on Physics-Informed Neural Networks (PINNs) is proposed to explore the operability space of a bubbling fluidized bed (BFB) plastic pyrolysis process. The approach integrates mechanistic knowledge through explicit mass balance constraints with data-driven learning, enabling accurate prediction of and feasibility boundaries. An adaptive sampling framework is employed to iteratively augment the training dataset. The trained PINN surrogate is then used to predict feasible regions and perform constrained optimization aimed at minimizing tar production, which is one of the most problematic byproducts in plastic pyrolysis processes. Beyond classical optimality, a robustness-oriented uncertainty quantification methodology is introduced, combining local perturbations with feasibility filtering to assess the reliability of the optimal solution. Quantitative robustness metrics, including relative objective uncertainty, feasibility retention ratio, and an overall robustness index, are introduced and used to track convergence and select the most reliable operating point. Results show that the proposed framework efficiently converges to accurate feasibility regions and identifies operating conditions that balance optimal performance with robustness against uncertainty. This work provides a methodology for physics-driven process optimization and operability analysis, with potential applicability to a wide range of complex energy and chemical systems.

Keywords: Plastics Recycling, Circular Economy, Surrogate Modelling, Pyrolysis, Data-driven Operability, Physics-Informed Neural Networks

INTRODUCTION

The rampant surge in plastic waste generation and lack of sustainable management practises have posed a substantial threat to the ecosystem and human health in the last two decades [1], and plastic waste production is projected to triple by 2050 reaching 1, 200 million metric tons [2]. Chemical recycling through advanced thermochemical technologies (ATTs), such as pyrolysis [3, 4], represent a promising pathway to tackle the plastic waste issue, allowing us to produce a broad spectrum of chemical feedstock for the manufacturing sector [5] and promoting the transition to a true circular economy [6, 7]. Plastics pyrolysis involves feedstock thermal decomposition at temperatures in the range of approximately 400 – 800 °C and in complete absence of oxidizing agents. This process promotes the formation of both gas and liquid products, whose relative amount depends on the reactor operating conditions. The pyrolysis gas is mainly composed of hydrogen and light hydrocarbons. After cleaning and refining, this gas can be used as chemical feedstock by the manufacturing industry. The liquid product, also known as pyrolysis oil, can be upgraded and used to produce olefins, paraffins and substitute fuels. To achieve these results, bubbling fluidized bed reactors (BFBR) are among the best reactor design for ATTs, due to their favourable operating flexibility, and enhanced heat and mass transfer [8]. However, when processing plastic waste, they are subject to hydrodynamic instabilities due to the plastic melting and unwanted byproducts formation, such as tar and waxes, that can lead to products quality deviations and even early plant shutdown if not properly monitored during operation. This challenge raises the urgency of developing reliable modelling approaches to control BFBR for chemical recycling, de-risking their implementation at industrial scale and improving their performance. While physics-based or mechanistic models are successfully used in the design stage of industrial chemical reactors, their integration for predicting product quality and controlling operations comes at significant computing costs. The opposite approach involves using fully data-driven models, which can ultimately lead to similar issues as they completely lack physical understanding of the process. This work proposes a combination of established process-specific semi-empirical approaches and physics-informed machine learning algorithms to optimize BFBR for chemical recycling of plastic waste. The objective of this work is to find the optimal operating conditions that minimize the yield of tar produced during pyrolysis and elucidate design space trade-offs [9, 10, 11].

A mechanistic model of a fluidized bed reactor for plastic waste pyrolysis is employed, based on kinetics semi-empirical correlations obtained from the literature [12]. This model predicts the yield of the main pyrolysis products, including volatile matter, tar and char, which represent unreacted carbon. Although this model is relatively simple, in general directly embedding pure mechanistic models within an optimisation framework is computationally prohibiting and this motivates the use of surrogate models [13, 14]. Using adaptive sampling, we develop a Physics-Informed Neural Network (PINN) as a surrogate [15, 16], by minimizing simultaneously data loss and physics loss. In this work, the physics loss enforces the conservation of mass between inlet and outlet of the BFBR. The use of neural networks for feasible region identification has already been proven successful, as highlighted by Metta et al. (2020) [17]. Finally, we use the trained PINN within an optimization framework to quantify maximum operability limits [18] and identify the optimal operating conditions that minimize the tar yield.

METHODOLOGY

Mechanistic model of plastic pyrolysis in BFB

A mechanistic model $\mathcal{M}$ for plastic pyrolysis in a bubbling fluidized bed reactor is employed to describe the relationship between reactor operating conditions and product yields. The model is based on semi-empirical correlations obtained by Vitale et. al (2024) [12], capturing the dependence of temperature on the yield of volatiles, tar and char during pyrolysis of polypropylene, as follows:

$$\boldsymbol{y}(F, T) = \boldsymbol{A}T + \boldsymbol{B} \tag{1}$$

Where $\boldsymbol{y}$ is the vector of volatiles, tar and char mass flow rates $\dot{m}$, and the hydrogen-to-methane mass ratio h in the pyrolysis gas (H_2/CH_4), while $\boldsymbol{A}$ and $\boldsymbol{B}$ are vectors of coefficients obtained from experimental data fitting. The parameter h is a key indicator of gas quality and it is considered in this work as one of the criteria to determine the feasible operability region.

Although the mechanistic model employed in this work consists of linear semi-empirical correlations that are computationally inexpensive, the primary objective of this study is to develop a general algorithmic strategy for feasibility discovery through adaptive sampling and robustness-driven design using PINN.

The reactor system inputs are the plastic feed flow rate F and operating temperature T, which also constitute the decision variables of the optimization problem. The BFB is considered to operate with nitrogen at twice the minimum fluidization condition. The set of operating conditions $\mathcal{D}$ of the BFB is given by the temperature range of 650 – 850 °C and the plastic feed mass flow rate range of 20 – 30 kg/h. The temperature limits are chosen in order to remain consistent with the experimental conditions used by the authors, while the flow rates are chosen to vary in a reasonable range for medium size BFB pyrolizers.

PINN surrogate model

A PINN is developed to act as a surrogate for the mechanistic BFB model. The PINN maps the reactor inputs F and T to the vector of outputs including volatiles, tar and char mass flow rates, and H_2/CH_4. The neural network consists of a fully connected feedforward architecture with 1 hidden layer of 20 neurons and hyperbolic tangent activation functions. Several authors observed that a single hidden layer is a good function approximator, provided sufficient number of hidden neurons [17]. The PINN is trained by minimizing a composite loss function including three contributions, as shown in the equation below: a data loss term, a physics loss term, and an L2 regularization term to avoid overfitting. The loss terms are calculated using a MSE metric.

$$\mathcal{L}(\theta) = \frac{1}{N}\sum_{i=1}^{N}\|\hat{y}_i - y_i\| + \frac{1}{N}\sum_{i=1}^{N}\left\|\hat{\dot{m}}_{out,i} - F_i\right\| + \lambda_{L2}\sum_k \theta_k \tag{2}$$

Where N are the collocation points in the domain, $\hat{y}$ is the PINN prediction, y is the output of the mechanistic model, λ_{L2} is the regularization weight, θ_k is the kth trainable parameter of the PINN, and $\hat{\dot{m}}_{out}$ and F are the overall mass flowrates at outlet and inlet of the BFB, respectively.

The physics loss enforces mass conservation by constraining the predicted outlet flow rate to match the inlet feed flow rate in real physical units. This constraint embeds first-principles knowledge into the learning process and improves extrapolation behavior in sparsely sampled regions of the operating space. Input and output variables are standardized prior to training to ensure numerical stability.

PINN-driven feasibility analysis

An initial training dataset of 100 points is generated using Latin Hypercube Sampling (LHS) over the predefined set of operating conditions for feed flow rate and reactor temperature. The corresponding mechanistic model outputs are used to initialize the PINN training. This initial step is summarized by the following equations:

$$\{x_i\}_{i=1}^{N_0} \sim LHS(\mathcal{D}) \tag{3}$$

$$y_i = \mathcal{M}(x_i) \tag{4}$$

To progressively improve surrogate accuracy in regions of interest, an adaptive sampling strategy is employed. At each adaptive iteration, the PINN is retrained using all available data, after which a dense pool of candidate points is generated within the operating conditions set using LHS. An acquisition function is defined and evaluated on this pool to identify new informative samples. The acquisition is chosen to encourage the PINN to learn regions with high physics residuals, where the surrogate violates mass conservation. The candidate point maximizing this acquisition function is selected, the corresponding output is evaluated using the mechanistic model and added to the training dataset. This approach encourages the PINN to learn regions of the space according to physics constrains. This is the main novelty aspect of the methodology developed in this work. The adaptive sampling algorithm at each iteration can be summarized by the following steps:

1. Train PINN

$$\theta = \arg\min_{\theta} \mathcal{L}(\theta) \tag{5}$$

2. Generate a dense pool of candidate points

$$\{\tilde{\mathbf{x}}_j\}_{j=1}^{N_c} \sim LHS(\mathcal{D}) \tag{6}$$

3. Evaluate surrogate and physics residual

$$r_j = |\hat{m}_{out}(\tilde{\boldsymbol{x}}_j) - \tilde{F}_j| \tag{7}$$

4. Evaluate acquisition function

$$a(\tilde{\boldsymbol{x}}_j) = \frac{r_j}{max(r)} \tag{8}$$

5. Select new sample

$$x_{new} = \arg\max_{\tilde{\boldsymbol{x}}_j} a(\tilde{\boldsymbol{x}}_j) \tag{9}$$

6. Update training dataset

$$\mathcal{D}_{k+1} = \mathcal{D}_k \cup \{x_{new}, \mathcal{M}(x_{new})\} \tag{10}$$

Subsequently, the process feasibility region is determined through a combination of physics and operational constraints, as follows:

$$\Omega = \left\{(F,T) \in \mathcal{D} \;\middle|\; \begin{matrix} r(F,T) \le \varepsilon \\ h_{min} \le \hat{h}(F,T) \le h_{max} \end{matrix} \right\} \tag{11}$$

The physics residual associated with mass conservation must remain below a prescribed tolerance. Moreover, the H_2/CH_4 is constrained to lie within a specified range, reflecting pyrolysis gas requirements for downstream utilization. The values of ε, h_{min} and h_{max} used to run the algorithm in this work are 1e-2, 0.4 and 0.6, respectively.

Optimization and sensitivity analysis

The trained PINN surrogate is embedded within a constrained optimization framework to identify operating conditions that minimize tar production while satisfying feasibility constraints. The optimal operating point is selected as the feasible point with minimum tar within the feasible region, as follows:

$$x^* = \arg\min_{(F,T)\in\Omega} \hat{m}_{tar}(x) \tag{12}$$

To quantify local uncertainty, a local perturbation analysis is performed on the optimum point. The perturbations were generated at each adaptive iteration from a normal distribution with zero mean, as follows:

$$\delta_p \sim \mathcal{N}(0, \sigma) \tag{13}$$

$$x_p^* = x^* + \delta_p \tag{14}$$

Where x_p^* is the p[th] perturbated optimum point. Each perturbated sample is evaluated using the PINN and it is retained if satisfies the same feasibility constraints shown in Eq. 11. If N_δ and N_{feas} are the number of perturbated samples and feasible perturbated samples for the tar mass flow rate, respectively, it is possible to define the following metrics:

$$FRR = \frac{N_{feas}}{N_\delta} \tag{15}$$

$$\sigma_{tar} = \frac{\Delta\hat{m}_{tar}}{\hat{m}_{tar^*}} \tag{16}$$

Where FRR is the feasibility retention ratio, σ_{tar} is the relative uncertainty of the optimal tar value, and $\Delta\hat{m}_{tar}$ and $\hat{m}_{tar}*$ are the 95% confidence interval (CI) for the outlet tar mass flow rate and the optimum tar mass flow rate, respectively. A high value of FRR indicates that small perturbations around the optimum remain feasible with high probability, while σ_{tar} captures the sensitivity of the objective value to local perturbations around the optimum. Finally, an overall robustness index can be calculated as:

$$RI = (1 - \sigma_{tar})\, FRR \tag{17}$$

This metric simultaneously rewards small tar uncertainty and high retention of feasible perturbations. The best feasibility region and optimum are chosen to be those with the highest value of RI.

A block diagram of the entire algorithm is shown in Figure 1.

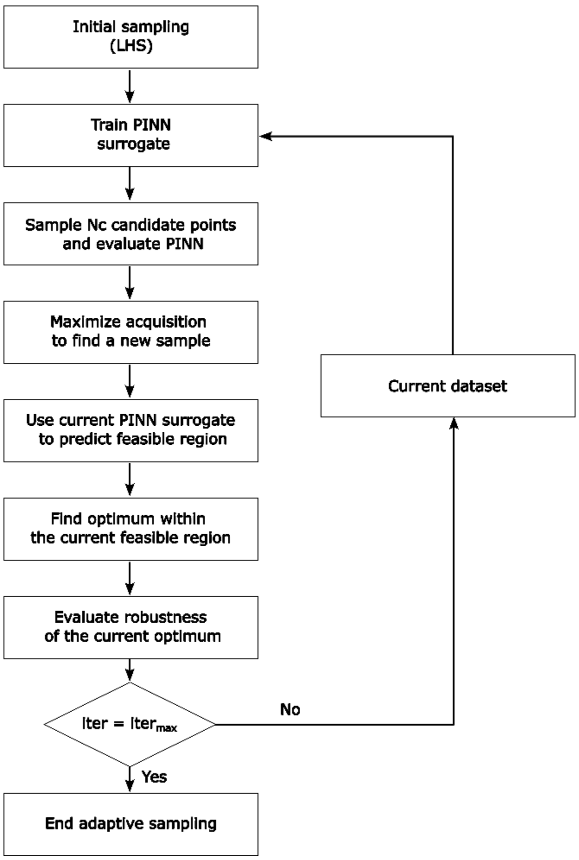

Figure 1. Adaptive sampling algorithm.

Table 1 presents the values of relevant parameters used to run the algorithm.

Table 1: Parameters used in this study.

Parameter	Description	Value/Name
F_{min}, F_{max}	Bounds of plastic mass feed flow rate	20 - 30 kg/h
T_{min}, T_{max}	Bounds of BFB temperature	650 - 850 kg/h
N_0	Number of initial design points (LHS)	100
N_c	Number of samples in the dense pool of candidate points (LHS)	5000
iter	Maximum number of adaptive sampling iterations	200
N_{layers}	Number of PINN hidden layers	1
$N_{neurons}$	Number of PINN hidden neurons	20
η	Learning rate for Adam optimizer	1e-3
N_{epochs}	Number of PINN training epochs	7000
ε	Mass balance residual tolerance	1e-2
h_{min}, h_{max}	Bounds of H_2/CH_4 ratio	0.4 – 0.6
N_δ	Number of perturbations per iteration	5000
σ	Standard deviation for perturbation	0.3

RESULTS AND DISCUSSION

Feasible region identification and optimum

Figure 2 compares the feasible operating regions and tar flow rate iso-contours obtained at two different stages of the adaptive sampling procedure: the last iteration (200 adaptive points) and the iteration corresponding to the maximum robustness index (191 adaptive points).

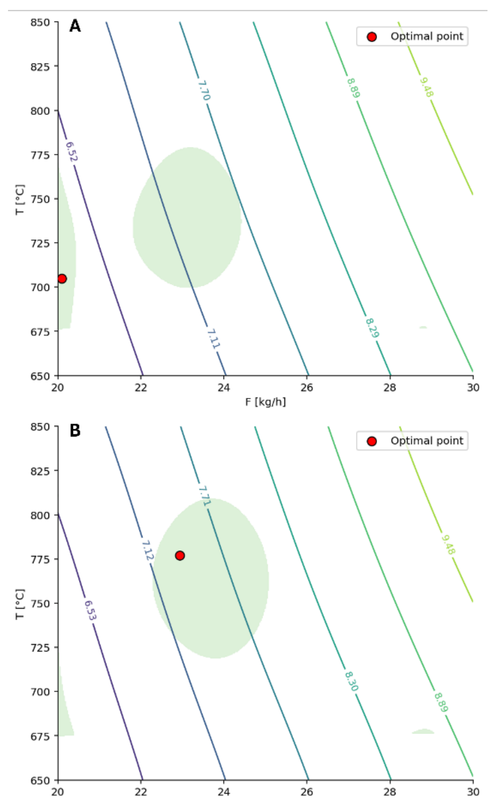

Figure 2. Feasible operating region with tar iso-contours and optimal point after 200 (A) and 191 adaptive samples (B).

Although both feasibility regions are obtained using the same PINN architecture and feasibility criteria, they reveal fundamentally different behaviors in terms of operability structure, and optimum point location. At the last iteration (Figure 2-A, iter = 200), the feasible region appears more fragmented, with greater disconnected areas. The shaded feasibility domain is narrow in the temperature direction. In contrast, at the robustness-optimal iteration (Figure 2-B, iter = 191), the feasible region shows smaller disconnected area at low feed flowrate values when compared with Figure 2-A. The smoother and more compact geometry suggests that the PINN has captured the feasibility constraints more consistently, resulting in a better-defined operating window. A key difference between the two figures lies in the location of the optimal operating point relative to the feasible region. In Figure 2-A, the optimal point lies very close to the feasibility boundary, particularly near the lower temperature and feed flow rate limits. In this case, even small uncertainties in the model predictions or minor disturbances in operating conditions could lead to constraint violation. However, in Figure 2-B, the optimal point is located farther from the boundary of the feasible region. This interior positioning provides a substantial operability margin, making the solution more resilient to uncertainty in process operation.

Perturbation and robustness analysis

Table 2 compares the robustness index RI and optimum for the two different adaptive sample numbers (191 and 200).

Table 2. Optimal solution and *RI* at the two iterations investigated.

Iteration	RI	Optimal values
191	0.538	$\hat{F}^* = 22.93\ kg/h$ $\hat{T}^* = 777.14$ °C $\widehat{m}_{tar}{}^* = 7.37$ kg/h $\hat{h}^* = 0.545$ $r = 2.96e-3$
200	0.157	$\hat{F}^* = 20.10\ kg/h$ $\hat{T}^* = 704.75$ °C $\widehat{m}_{tar}{}^* = 6.17$ kg/h $\hat{h}^* = 0.437$ $r = 3.13e-3$

The discussion in the previous section agrees with the values obtained for the RI. The robustness index integrates objective certainty and feasibility retention into a single metric, and its values are 0.157 and 0.538 at iteration 200 and 191, respectively. Figure 3 compares the uncertainty boundaries obtained by perturbing the optimal operating point identified at the iteration with the highest robustness index and at the final adaptive iteration. Each one represents feasible operating points generated by local perturbations around the nominal optimum and filtered by feasibility constraints as explained in the Methodology section, providing a direct visualization of local operability robustness.

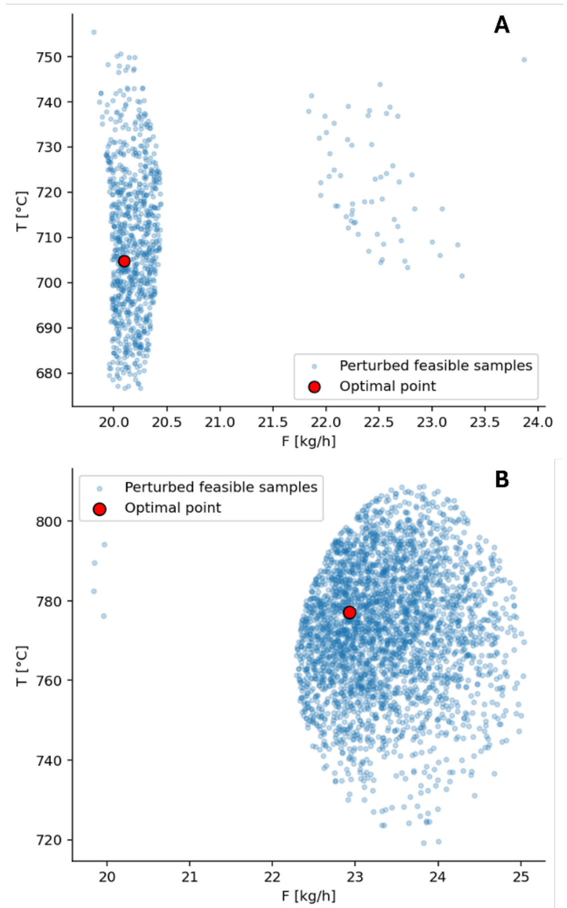

Figure 3. Optimum and feasible perturbed points after 200 (A) and 191 adaptive samples (B).

For the best-robustness iteration (Figure 3-B), feasible perturbations are more densely distributed around the optimum, indicating that small variations in feed rate and temperature may not readily violate feasibility constraints. In contrast, the final iteration exhibits a markedly different perturbation pattern (Figure 3-A). The feasible samples form a narrow, elongated region, particularly constrained in the feed rate dimension. While feasibility is retained under some perturbations, the admissible region collapses rapidly along one coordinate, suggesting that the optimal point lies close to a constraint. This explains the lower robustness index observed at the final iteration. Despite further adaptive refinement of the surrogate, this indicates increased sensitivity of feasibility to small input variations and highlights the risk of operating near constraint boundaries, even when the objective value appears to be favorable.

These results emphasize that continued adaptive sampling does not necessarily improve operational robustness but can lead to over-refinement around feasibility boundaries. While later iterations may sharpen these boundaries or marginally improve objective values, they can also drive the optimizer toward regions of higher sensitivity. Whereas the iteration with the highest robustness index achieves the best trade-off between performance and reliability.

CONCLUSIONS

This work presents a novel physics-informed strategy based on PINNs to explore the design space and predict the feasibility region for a BFB pyrolysis process. Optimization and sensitivity analysis are also performed to find the optimum operating point, as well as investigate its robustness. By embedding fundamental mass balance constraints directly into the learning process, the proposed PINN framework achieves physically consistent predictions while maintaining flexibility in data-driven modeling. The introduction of an adaptive sampling scheme enables efficient exploration of the input space, progressively refining the surrogate model in regions of high violation of the mass balance constraint. This results in accurate operability maps that capture complex feasible regions without requiring exhaustive mechanistic simulations. A key contribution of this study is the explicit integration of robustness analysis into the optimization workflow. Local perturbations around candidate optima are used to quantify uncertainty in both operating variables and objective values, while feasibility filtering ensures that robustness is evaluated under strict process constraints. The combined use of relative objective uncertainty and feasibility retention ratio allows the definition of a robustness index that discriminates between purely optimal solutions and those that are reliably operable under uncertainty. The comparison between early and late adaptive iterations highlights that continued sampling does not necessarily improve robustness, highlighting the importance of robustness-aware criteria. The results show that the most robust operating point may emerge before full convergence of the feasible region, offering practical insights for reducing computational effort while maintaining reliability.

Overall, the proposed methodology provides a framework for feasibility prediction, constrained optimization, and robustness assessment in complex thermochemical systems. Its modular structure and physics-informed features make it readily extendable to higher-dimensional design spaces, additional constraints, and alternative reactor configurations. As this study is a proof of concept based on a semi-empirical literature model, its industrial applicability is currently limited. Future works should be directed towards validation using experimental and plant data.

ACKNOWLEDGEMENTS

The authors would like to acknowledge EPSRC and UK Research and Innovation (UKRI) for funding this research project. Grant numbers: UKRI787, EP/V051008/1, EP/W003317/1.

AUTHOR IDENTIFIERS

Author ORCIDs:
Iannello S: 0000-0001-7894-398X
Charitopoulos V.M.: 0000-0001-9051-917X
Materazzi M: 0000-0001-6350-2559

REFERENCES

1. OECD (2022), Global Plastics Outlook. https://www.oecd.org/en/publications/2022
2. Badejo O, Hernández B, Ierapetritou M. Design of the transition for sustainable plastic waste management under carbon policies in the united states. Ind. Eng. Chem. Res. 64:5476-5492 (2025). https://doi.org/10.1021/acs.iecr.4c03942
3. Crîstiu D, d'Amore F, Bezzo F. Economic and environmental optimisation of mixed plastic waste supply chains in northern italy comparing incineration and pyrolysis technologies. Computers & Chemical Engineering 180:108503 (2024). https://doi.org/10.1016/j.compchemeng.2023.108503
4. García RC, Erickson ED, Martín M, Zavala VM. Evaluating the potential of plastic waste upcycling using thermochemical technologies: a case study in spain. Computers & Chemical Engineering 206:109524 (2026). https://doi.org/10.1016/j.compchemeng.2025.109524
5. Chari S, Sebastiani A, Paulillo A, Materazzi M. The environmental performance of mixed plastic waste gasification with carbon capture and storage to produce hydrogen in the U.K.. ACS Sustainable Chem. Eng. 11:3248-3259 (2023). https://doi.org/10.1021/acssuschemeng.2c05978
6. Avraamidou S, Baratsas SG, Tian Y, Pistikopoulos EN. Circular economy - a challenge and an opportunity for process systems engineering. Computers & Chemical Engineering 133:106629 (2020). https://doi.org/10.1016/j.compchemeng.2019.106629
7. Nixon KD, Schyns ZOG, Luo Y, Ierapetritou MG, Vlachos DG, Korley LTJ, Epps, III TH. Analyses of circular solutions for advanced plastics waste

recycling. Nat Chem Eng 1:615-626 (2024). https://doi.org/10.1038/s44286-024-00121-6
8. Iannello S, Morrin S, Materazzi M. Fluidised bed reactors for the thermochemical conversion of biomass and waste. KONA 37:114-131 (2020). https://doi.org/10.14356/kona.2020016
9. Pistikopoulos EN, Tian Y, Bindlish R. Operability and control in process intensification and modular design: challenges and opportunities. AIChE Journal 67: (2021). https://doi.org/10.1002/aic.17204
10. Sachio S, Kontoravdi C, Papathanasiou MM. A model-based approach towards accelerated process development: a case study on chromatography. Chemical Engineering Research and Design 197:800-820 (2023). https://doi.org/10.1016/j.cherd.2023.08.016
11. Tian H, Ierapetritou MG. A surrogate?based framework for feasibility?driven optimization of expensive simulations. AIChE Journal 70: (2024). https://doi.org/10.1002/aic.18364
12. Vitale A, Di Carlo A, Foscolo PU, Papa AA. Kinetic model implementation of fluidized bed devolatilization. Energies 17:3154 (2024). https://doi.org/10.3390/en17133154
13. Scelfo G, Charitopoulos VM, Vicari F, Tamburini A, Bogle DI, Micale G, Cipollina A. Surrogate-based optimization analysis and scale-up of an ultra-concentrated brine pilot treatment chain for sustainable mineral recovery. Desalination 621:119682 (2026). https://doi.org/10.1016/j.desal.2025.119682
14. Misener R, Biegler L. Formulating data-driven surrogate models for process optimization. Computers & Chemical Engineering 179:108411 (2023). https://doi.org/10.1016/j.compchemeng.2023.108411
15. Cai S, Mao Z, Wang Z, Yin M, Karniadakis GE. Physics-informed neural networks (pinns) for fluid mechanics: a review. Acta Mech. Sin. 37:1727-1738 (2022). https://doi.org/10.1007/s10409-021-01148-1
16. Iannello S, Friso A, Galvanin F, Materazzi M. A hybrid physics–machine learning approach for modeling plastic–bed interactions during fluidized bed pyrolysis. Energy Fuels 39:4549-4564 (2025). https://doi.org/10.1021/acs.energyfuels.4c05870
17. Metta N, Ramachandran R, Ierapetritou M. A novel adaptive sampling based methodology for feasible region identification of compute intensive models using artificial neural network. AIChE Journal 67: (2020). https://doi.org/10.1002/aic.17095
18. Meng Q, Bogle D, Charitopoulos VM. Probabilistic design space exploration and optimization via bayesian approach for a fluid bed drying process. European Journal of Pharmaceutical Sciences 210:107116 (2025). https://doi.org/10.1016/j.ejps.2025.107116